

We are IntechOpen, the world's leading publisher of Open Access books Built by scientists, for scientists

6,900

Open access books available

186,000

International authors and editors

200M

Downloads

Our authors are among the

154

Countries delivered to

TOP 1%

most cited scientists

12.2%

Contributors from top 500 universities



WEB OF SCIENCE™

Selection of our books indexed in the Book Citation Index
in Web of Science™ Core Collection (BKCI)

Interested in publishing with us?
Contact book.department@intechopen.com

Numbers displayed above are based on latest data collected.
For more information visit www.intechopen.com



Magnetic Properties of Transition-Metal-Doped Silicon Carbide Diluted Magnetic Semiconductors

Andrei Los^{1,2} and Victor Los³

¹ISS Ltd., Semiconductors and Circuits Lab

²Freescale Semiconductor Ukraine LLC

³Institute of Magnetism, National Academy of Sciences
Kiev, Ukraine

1. Introduction

Possibility to employ the spin of electrons for controlling electronic device operation has long been envisaged as a foundation for future extremely low power amplifying and logic devices, polarized light emitting diodes, new generation magnetic field sensors, high density 3D magnetic memories, etc. (Gregg et al., 2002; Žutić et al., 2004; Bratkovsky, 2008). While metal-metal and metal-insulator spin-electronic (or spintronic) devices have already found their application as hard drive magnetic field sensors and niche nonvolatile memories, diluted magnetic semiconductors (DMSs), i.e. semiconductors with a fraction of the atoms substituted by magnetic atoms, are expected to become a link enabling integration of spin-electronic functionality into traditional electron-charge-based semiconductor technology. Following the discovery of carrier-mediated ferromagnetism due to transition metal doping in technologically important GaAs and InAs III-V compound semiconductors (Munekata et al., 1989; Ohno et al., 1996), a wealth of research efforts have been invested in the past two decades into investigations of magnetic properties of DMSs. Ferromagnetic semiconductors were, of course, not new at the time and carrier-mediated ferromagnetism, a lever allowing electrical control of the magnetic ordering, had also been demonstrated albeit only at liquid helium temperatures (Pashitskii & Ryabchenko, 1979; Story et al., 1986). The achievement of the ferromagnetic ordering temperature, the Curie temperature T_C , in excess of 100 K in (Ga, Mn) As compounds was a significant step towards practical semiconductor spintronic device implementation. A substantial progress has been achieved in increasing the ordering temperature in this material system and T_C as high as 180 K has been reported (Olejník et al., 2008). (Ga, Mn) As has effectively become a model magnetic semiconductor material with its electronic, magnetic, and optical properties understood most deeply among the DMSs. Still, however, one needs the Curie temperature to be at or above room temperature for most practical applications.

Mean-field theory of ferromagnetism (Dietl et al., 2000; Dietl et al., 2001), predicting that above room temperature carrier-mediated ferromagnetic ordering may be possible in certain wide bandgap diluted magnetic semiconductors, including a family of III-nitrides and ZnO, had spun a great deal of interest to magnetic properties of these materials. The resulting

flurry of activities in this area led to apparent early successes in fabricating the DMS samples exhibiting ferromagnetism above room temperature (Pearton et al., 2003; Hebard et al., 2004). Ferromagnetic ordering in these samples was attributed to formation of homogeneous DMS alloys which, however, was in many cases later refuted and explained differently, by, for instance, impurity clustering, at the time overlooked by standard characterization techniques. Much theoretical understanding has been gained since then on the effects of exchange interaction, self-compensation, spinodal decomposition, etc. Given that various effects may mimic the “true DMS” behaviour, a careful investigation of the microscopic picture of magnetic moments formation and their interaction, as well as attraction of different complementary experimental techniques is required for a realistic understanding and prediction of the properties of this complex class of materials.

Silicon carbide is another wide bandgap semiconductor which has been considered a possible candidate for spin electronic applications. SiC has a long history of material research and device development and is already commercially successful in a number of applications. The mean field theory (Dietl et al., 2000; Dietl et al., 2001) predicted that semiconductors with light atoms and smaller lattice constants might possess stronger magnetic coupling and larger ordering temperatures. Although not applied directly to studying magnetic properties of SiC, these predictions make SiC DMS a promising candidate for spintronic applications.

Relatively little attention has been paid to investigation of magnetic properties of SiC doped with TM impurities, and the results obtained to date are rather modest compared to many other DMS systems and are far from being conclusive. Early experimental studies evidenced ferromagnetic response in Ni-, Mn-, and Fe-doped SiC with the values of the Curie temperature T_C varying from significantly below to close to room temperature (Theodoropoulou et al., 2002; Syväjärvi et al., 2004; Stromberg et al., 2006). The authors assigned the magnetic signal to either the true DMS behaviour or to secondary phase formation. Later experimental reports on Cr-doped SiC suggested this material to be ferromagnetic with the $T_C \sim 70$ K for Cr concentration of ~ 0.02 wt% (Huang & Chen, 2007), while above room temperature magnetism with varying values of the atomic magnetic moments was observed for Cr concentration of 7-10 at% in amorphous SiC (Jin et al., 2008). SiC doped with Mn has become the most actively studied SiC DMS material. Experimental studies of Mn-implanted 3C-SiC/Si heteroepitaxial structure (Bouziane et al., 2009), of C-incorporated Mn-Si films grown on 4H-SiC wafers (Wang et al., 2007), a detailed report by the same authors on structural, magnetic, and magneto-optical properties of Mn-doped SiC films prepared on 3C-SiC wafers (Wang et al., 2009) as well as studies of low-Mn-doped 6H-SiC (Song et al., 2009) and polycrystalline 3C-SiC (Ma et al., 2007) all suggested Mn to be a promising impurity choice for achieving high ferromagnetic ordering temperatures in SiC DMS. Researchers recently turned to studying magnetic properties of TM-doped silicon carbide nanowires (Seong et al., 2009).

Theoretical work done in parallel in an attempt to explain the available experimental data and to obtain guidance for experimentalists was concentrated on first principles calculations which are a powerful tool for modelling and predicting DMS material properties. Various *ab initio* computational techniques were used to study magnetic properties of SiC DMSs theoretically. Linearized muffin-tin orbital (LMTO) technique was utilized for calculating substitution energies of a number of transition metal impurities in 3C-SiC (Gubanov et al., 2001; Miao & Lambrecht, 2003). The researchers found that Si site is more favourable

compared to C site for TM substitution. This result holds when lattice relaxation effects are taken into account in the full-potential LMTO calculation. Both research teams found that Fe, Ni and Co were nonmagnetic while Cr and Mn possessed nonzero magnetic moments in the 3C-SiC host. Calculation of the magnetic moments in a relaxed supercell containing two TM atoms showed that both Mn and Cr atoms ordered ferromagnetically. Ferromagnetic ordering was later confirmed for V, Mn, and Cr using ultrasoft pseudopotential plane wave method (Kim et al., 2004). In another *ab initio* study, nonzero magnetic moments were found for Cr and Mn in 3C-SiC using full potential linearized augmented plane wave (FLAPW) calculation technique and no relaxation procedure accounting for impurity-substitution-related lattice reconstruction (Shaposhnikov & Sobolev, 2004). The authors additionally studied magnetic properties of TM impurities in 6H-SiC substituting for 2% or 16% of host atoms. It was found that on Si site in 6H-SiC Cr and Mn possessed magnetic moments in both concentrations, while Fe was magnetic only in the concentration of 2%. Ultrasoft pseudopotentials were used for calculations of magnetic moments and ferromagnetic exchange energy estimations for the case of Cr doping of 3C-SiC (Kim & Chung, 2005). In a later reported study (Miao & Lambrecht, 2006) the authors used FP-LMTO technique with lattice relaxation to compare electronic and magnetic properties of 3C- and 4H-SiC doped with early first row transition metals. Spin polarization was found to be present in V, Cr, and Mn-doped SiC. The authors of (Bouziane et al., 2008) additionally studied the influence of implantation-induced defects on electronic structure of Mn-doped SiC. The results of the cited calculations were also somewhat sensitive to the particular calculation technique employed.

Here, we attempt to create a somewhat complete description of SiC-based diluted magnetic semiconductors in a systematic study of magnetic states of first row transition metal impurities in SiC host. Improving prior research, we do this in the framework of *ab initio* FLAPW calculation technique, perhaps one of the most if not the most accurate density functional theory technique at the date, combined with a complete lattice relaxation procedure at all stages of the calculation of magnetic moments and ordering temperatures. Accounting for the impurity-substitution-caused relaxation has been found crucial by many researchers for a correct description of a DMS system. We therefore are hopefully approaching the best accuracy of the calculations possible with the ground state density functional theory. We analyze the details of magnetic moments formation and of their change with the unit cell volume, as well as of the host lattice reconstruction due to impurity substitution. Such analysis leads to revealing multiple magnetic states in TM-doped SiC. We also study, for the first time, particulars of exchange interaction for different TM impurities and provide estimates of the magnetic ordering temperatures of SiC DMSs.

2. Methodology and computational setup

2.1 SiC-TM material system

Crystal lattice of any SiC polytype can be represented as a sequence of hexagonal close-packed silicon-carbon bilayers. Different bilayer stacking sequences correspond to different polytypes. For example, for the most technologically important hexagonal 4H polytype, the stacking sequence is ABAC (or, equivalently, ABCB), where A, B, and C denote hexagonal bilayers rotated by 120° with respect to each other (Bechstedt et al., 1997). The stacking sequence for another common polytype, the cubic 3C-SiC, is ABC. Although in all SiC

polytypes the nearest neighbours of any Si or C atom are always four C or Si atoms, respectively, forming tetrahedra around the corresponding Si or C atom, there are two types of the sites (and layers) in SiC lattice, different in their next nearest neighbour arrangement or the medium range order. The stacking sequences for these different sites are ABC and ABA, where in the former the middle layer (layer B) has the cubic symmetry (sometimes also called quasi-cubic if one deals with such layer in a hexagonal polytype), while in the latter the symmetry of the middle layer is hexagonal (Bechstedt et al., 1997). There are only cubic layers in 3C-SiC, while other common polytypes such as 4H and 6H contain different numbers of both hexagonal and cubic layers. We will show below that site symmetry plays crucial role in TM d-orbital coupling and, therefore, ferromagnetic ordering temperatures of SiC DMSs.

Diluted magnetic semiconductor material systems usually have TM impurity concentrations of the order of several atomic per cent. Such concentrations, although very high for typical semiconductor device applications, are essential for securing efficient exchange interaction between TM impurities and thus achieving high ordering temperatures needed for practical spintronic device operation. In our calculations of the magnetic properties of SiC DMSs the effective TM impurity concentrations range from about 4% to 10%. Substitutional TM impurity in the host SiC lattice is assumed to reside at the Si sites in the SiC crystal lattice. The choice of the substitution site preference can be made according to the atomic radii which are much closer for Si and TM than for C and TM and, therefore, much smaller lattice distortion would be required in the case of Si site substitution. Results of prior studies of the TM substitution site preference (Gubanov et al., 2001; Miao & Lambrecht, 2003) support this intuitive approach.

It is important that the Fermi level position in a semiconductor system with diluted TM doping of several per cent is defined by the TM impurity itself, unless another impurity is present in the system in a comparable concentration. In other words, in such a DMS system, TM impurity pins the Fermi level and defines its own charge state and charge states of all other impurities. From the computational point of view this is, of course, automatically achieved by the self-consistent solution for the state occupation. If one were to vary the TM impurity charge state independently, this would require co-doping with a comparable amount of another donor or acceptor. On the other hand, reducing TM concentration to the typical heavy doping levels of, say, 10^{19} cm^{-3} would result in an “ultradiluted magnetic semiconductor”, where an efficient exchange interaction would be hindered by large distances between the transition metal atoms, and this latter case is not considered here. Calculations of formation energies of different charge states of first row TM impurities in SiC (Miao & Lambrecht, 2003; Miao & Lambrecht, 2006) in their typical DMS concentrations indicate that they are expected to form deep donor and acceptor levels in the SiC bandgap, and be in their neutral charge states. This means that, contrary to the case of, for example, GaAs, TM impurities in SiC do not contribute free carriers which could mediate exchange interaction between the TM atoms.

2.2 Supercells

In this work, magnetic properties of TM-doped SiC are studied for 3C (Zincblende) and 4H (Wurtzite) SiC polytypes. We start with calculations of the lattice parameters and electronic structure of pure 3C- and 4H-SiC. The primitive cell of pure cubic 3C-SiC consists of single silicon-carbon pair. Another way of representing this type of lattice is with a sequence of

hexagonal close-packed Si-C bilayers with the ABC stacking sequence. In that case the unit cell consists of 3 Si-C bilayers or 6 atoms. Both cells are, of course, equivalent from the computational point of view and must produce identical results. The unit cell of 4H-SiC consists of 4 Si-C bilayers or 8 atoms.

Then, the lattice parameters, electronic structure and magnetic properties are calculated for 3C- and 4H-SiC doped with TM impurity. In the calculations, to model the lattice of doped single crystal SiC, we employ the supercell approach. For a doped semiconductor, the minimum lattice fragment (the supercell), needed to model the material, includes one impurity atom, while the total number of atoms in the supercell is inversely proportional to the impurity concentration. For only one TM atom in the supercell, the solution sought will automatically be a ferromagnetically-ordered DMS (in case a nonzero magnetic moment is obtained on TM atoms), as the solution is obtained for an infinite lattice implicitly constructed from the supercells with identically oriented magnetic moments. This is convenient and sufficient for establishing the trends for achieving spin polarization in the SiC-TM system. Investigation of true (energetically more preferable) magnetic moment ordering type requires larger supercells with at least two TM atoms with generally different directions of their magnetic moments.

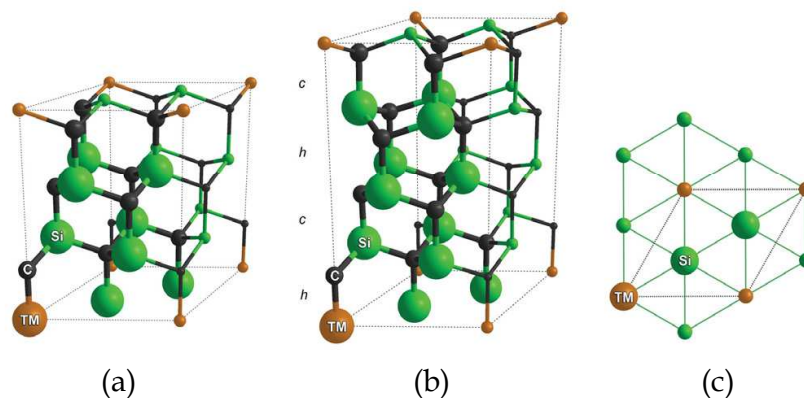


Fig. 1. Supercells of TM-doped (a) 3C-SiC and (b) 4H-SiC, and (c) in-plane TM atom placement used in the calculations of magnetic moments and properties of different magnetic states. TM, Si, and C atoms added by periodicity and not being part of the supercells are shown having smaller diameters compared to the similar atoms in the supercells. Layers with the hexagonal and quasicubic symmetries in 4H-SiC are marked by h and c , respectively.

Investigation of the magnetic moment formation and related lattice reconstruction in SiC doped with TM impurities is done using $\text{Si}_8\text{C}_9\text{TM}$ and $\text{Si}_{11}\text{C}_{12}\text{TM}$ supercells, containing a total of 18 and 24 atoms for 3C- and 4H-SiC, respectively. These supercells are shown in Fig. 1. Impurity atoms are placed in the centres of the adjacent close-packed hexagons, so that the distance between them equals $\sqrt{3}a$. In the c -axis direction, the distance between TM atoms is equal to one 3C or 4H-SiC lattice period (3 or 4 Si-C bilayers). The resultant impurity concentration calculated with respect to the total number of atoms is about 4 % in the case of 4H-SiC and about 5% in the case of 3C-SiC. As already mentioned, such concentrations are typical for experimental, including SiC, DMS systems.

Calculations of SiC DMS ordering temperatures require adding another TM impurity atom to the supercells. These supercells are shown in Fig. 2. In the case of 3C-SiC, we study magnetic ordering for two different spatial configurations of TM impurities in the SiC lattice. First, we simply double the 3C-SiC supercell shown in Fig. 1 in the c -direction so that the two TM atoms are at the distance of 14.27 a.u., while TM concentration is kept at 5 at % (Fig. 2 (a)). Next, we return to the original $\text{Si}_8\text{C}_9\text{TM}$ supercell and introduce an additional TM atom as the nearest neighbor to the TM atom in the Si-TM plane (Fig. 2 (b)). The distance between the TM atoms in this case equals to 5.82 a.u. and their effective concentration is approximately 10%. Such TM configuration can also be thought of as a simplest TM nanocluster in SiC lattice. For Mn-doping, which we identify as the most promising for obtaining high temperature SiC DMS, we additionally study substitution of a pair of TM atoms at different, hexagonal and cubic, 4H-SiC lattice sites with varying distances between the impurities and impurity electronic orbital mutual orientations (Fig. 2 c-e). We show that the strength of exchange coupling and the Curie temperature depend not only on the distance between TM atoms but also significantly on the particular lattice sites the impurities substitute at.

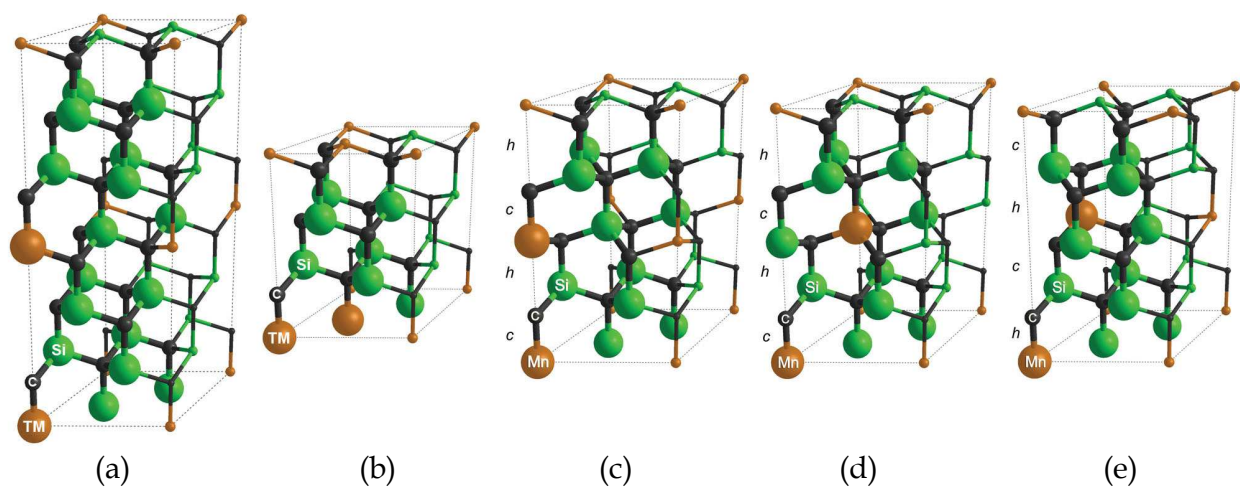


Fig. 2. SiC-TM supercells containing two TM atoms, which are used in the calculations of DMS ordering types and temperatures. Supercells (a) and (b) correspond to 3C-SiC, while supercells (c)-(e) correspond to 4H-SiC. TM, Si, and C atoms added by periodicity and not being part of the supercells are shown having smaller diameters compared to the similar atoms in the supercells. Layers with the hexagonal and quasicubic symmetries in 4H-SiC are marked by h and c , respectively.

2.3 Computational procedure

In contrast to earlier studies of magnetic properties of TM-doped SiC, the calculations are done for the supercells with optimized volumes and atomic positions, i.e. with both the local and global lattice relaxations accounted for. As we will show below, not only the FM ordering temperature, but also the value and even the existence of the magnetic moments in TM-doped semiconductor sensitively depend on the semiconductor host lattice structure and its reconstruction due to impurity substitution. Furthermore, it will be shown that multiple states with different, including zero, magnetic moments can be characteristic for SiC DMSs (and, perhaps, the other DMS systems as well). The different states correspond to

different equilibrium lattice configurations, transition between which involves reconstruction of the entire crystalline lattice. The reconstruction and the transition between the states may either be gradual or the states can be separated by an energy gap with the energy preference for either the magnetic or nonmagnetic state. The width of the energy gap between the different states varies across the range of impurities.

In the procedure, which is used for finding the optimized supercells, total energies are calculated for a number of volumes of isotropically expanded supercells. Additionally, at each value of the volume, the supercells are fully relaxed to minimize the intra-cell forces. Total energy-volume relationships for the relaxed supercells are then fitted to the universal equation of state (Vinet et al., 1989), and the minimum of the fitted curve corresponds to the supercell with the equilibrium volume and atomic positions in one of the magnetic states peculiar to that particular DMS. The supercells with such optimized equilibrium volumes and atomic positions are then used in the calculations of the DMS magnetic moments and ordering temperatures.

SiC DMS ordering type, either ferromagnetic (FM) or antiferromagnetic (AFM), and the corresponding values of the Curie or Néel critical temperatures are estimated from the total energy calculations for supercells containing a pair of TM impurities with their magnetic moments aligned in parallel (FM) or antiparallel (AFM). Employing the Heisenberg model, which should describe the orientational degrees of freedom accurately, for the description of the magnetic ordering, one can use the difference ΔE_{FM-AFM} between the total energies of the FM- and AFM-ordered supercells for estimating the value of the Curie or Néel temperature in the framework of the mean-field model using the following expression:

$$T_C = -\frac{1}{3k_B} \Delta E_{FM-AFM}, \quad (1)$$

where k_B is the Boltzmann constant. For the negative total energy difference ΔE_{FM-AFM} between the FM and AM states, the energy preference is for the FM state and (1) provides the Curie temperature value. When ΔE_{FM-AFM} is positive, the ground state of the DMS is AFM and the negative value of the critical temperature can be interpreted as the positive Néel temperature.

We note that the total energies of the FM and AFM states entering equation (1) are those of a simple ferromagnet and a two-sublattice Néel antiferromagnet models, describing only the nearest neighbour magnetic moment interactions. Taking into account the next neighbour interactions may result, particularly, in more complex, compared to the simple FM or AFM state, magnetic moment direction configurations. Using larger supercells with more TM atoms and taking into account more terms in the Heisenberg Hamiltonian would allow going beyond the model given by (1) and make the estimate of T_C more accurate. This, however, would lead to significantly larger computational resource requirements and is beyond the scope of the present work. The use of the simplest model is justified by the fact that usually the more long-range interactions of magnetic moments are noticeably weaker than the interactions between the nearest neighbours due to the rather localized nature of electronic shells responsible for the magnetic properties of TM atoms, as we will see below. It is important that, since the calculations are done in the framework of the ground state density functional theory, only direct TM-TM exchange mechanisms can be accounted for in this case. Another important type of exchange interaction which, for example, is peculiar to

Mn-doped GaAs, namely free-carrier-mediated exchange, requires attraction of different computational techniques for its modelling. We also note that since the calculated FM and AFM total ground state energies in (1) are defined by the electronic density distribution, which also defines the corresponding magnetic moment values, one can in general expect magnetic moments to be different in the FM and AFM states (see Table 3 and discussion below).

According to Eq. (1), the difference in the total energy values between the FM and AFM states corresponding to a Curie or Néel temperature change of, say, 50 K is about 14 meV per pair of TM atoms (per supercell). The accuracy of the total energy calculations needs to be better than this and per atom accuracy requirement, which is usually specified in the total energy calculations, is more strict for larger supercells or, equivalently, smaller impurity concentrations; this also means that critical temperature estimations for DMSs with smaller TM concentrations are typically prone to larger errors. Additionally, as will be evident from the discussion below, we need to resolve magnetic and nonmagnetic solutions which are close on the energy scale, and thus the accuracy of the calculations needs to be higher than at least the differences in energy between these solutions. To satisfy these accuracy requirements we perform both stringent convergence tests with respect to all parameters influencing the calculations and choose the corresponding settings for the self-consistent calculations convergence criteria.

The calculations are performed using the FLAPW technique (Singh & Nordstrom, 2006) implemented in the Elk (formerly EXCITING) software package (Dewhurst et al., 2004). Exchange-correlation potential is calculated using the generalized gradient approximation according to the Perdew-Burke-Ernzerhof model (Perdew et al., 1996). The muffin-tin radii are set at 2.0 a.u. for Si and TM atoms and 1.5 a.u. for C atoms. The APW basis set includes 150 plane waves per atom. Within the atomic spheres, spherical harmonic expansions with angular momentum up to 8 are used for the wave function, charge density, and potential representation. Local orbitals are added to the APW basis set to improve convergence and accuracy of the calculations. The self-consistent calculations are performed for 12 (Fig. 1, Fig. 2 (b)), 6 (Fig. 2 (a)), 8 (Fig. 2 (c)) and 10 (Fig. 2 (d) and (e)) reciprocal lattice points in the irreducible wedge of the Brillouin zone and are considered converged when the RMS change in the effective potential is less than 10^{-6} and the total energy error is within 0.1 meV/atom.

To check the computational setup, lattice constants of undoped 3C-SiC were obtained using the optimization procedure described above. The calculated unit cell volume was found to be equal to 70.19 a.u.³/atom. This is in an excellent agreement with the experimental value of 69.98 a.u.³/atom (Bechstedt et al., 1997) confirming the effectiveness of the lattice optimization procedure used. Calculated indirect bandgap of 3C-SiC of about 1.62 eV is below the experimental value of approximately 2.3 eV. Such bandgap underestimation is known to be a problem of the ground state density functional theory, in particular when LDA or GGA exchange-correlation functionals are used. Other carefully constructed exchange-correlation functionals may rectify the problem somewhat (Sharma et al., 2008). We, however, warn the reader from taking the DFT bandgap values literally.

3. Multiple magnetic states of TM-doped SiC

3.1 Magnetic moment formation and lattice reconstruction

We begin the discussion of different magnetic states, which can be created by a TM impurity in SiC, with the case of Fe-doped SiC. Calculated total energies of (Si, Fe) C supercells as a function of the supercell volume for 3C- and 4H-SiC are presented in Fig. 3 (a). Two equilibrium solutions were found for the total energy – supercell volume dependencies, one of which is characterized by a nonzero supercell magnetic moment, while in the other the supercell is nonmagnetic. The magnetic state possesses a larger total energy, while the nonmagnetic state is the ground state in Fe-doped 3C- and 4H-SiC. The total energy difference between the nonmagnetic and magnetic states at equilibrium volume is approximately 33 meV/atom in 3C-SiC and 20 meV/atom in 4H-SiC. Magnetic moment of Fe in the magnetic state changes approximately linearly from about 1.9 to 2.3 μ_B per Fe in the range of the volumes from about 68 a.u.³/atom to 78 a.u.³/atom (see Fig. 5 below). It is important to note that the two solutions were not obtained in a constrained magnetic moment calculation. Rather, the calculations converge to the magnetic solution if starting from a sufficiently expanded lattice. The nonmagnetic solution is obtained in the lattice with the unit cell volume approximately corresponding to undoped SiC. Both total energy – supercell volume curves are obtained by using the solution at each volume value as the initial approximation for the next one. Thus, we let the calculations naturally follow the underlying physical processes.

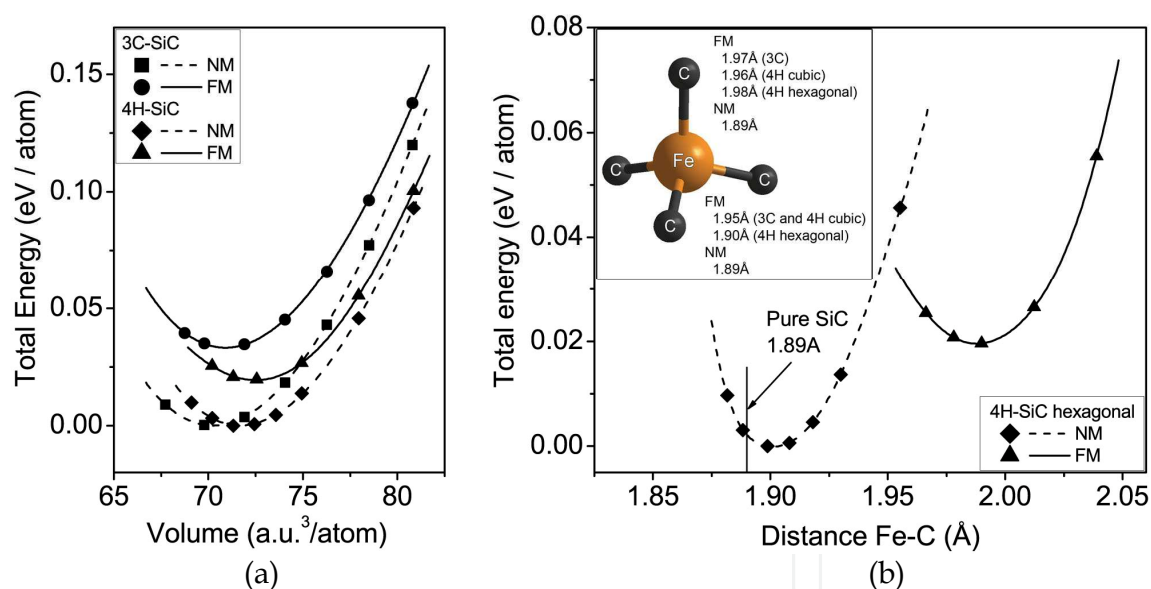


Fig. 3. Total energy – supercell volume dependencies for Fe-doped 3C- and 4H-SiC in the nonmagnetic and magnetic states (a). Fe-C bond length relaxation in the different states for C atom above Fe atom at the hexagonal lattice site in 4H-SiC (b). The inset shows tetrahedron relaxation details in different SiC polytypes and at lattice sites with different symmetries.

Crystal lattice of (Si, Fe) C DMS in its magnetic state is significantly reconstructed compared both to (Si, Fe) C in its nonmagnetic state and to undoped SiC. Lattice relaxation of the (Si, Fe) C supercell in its nonmagnetic state is minimal compared to undoped SiC. It is important that the magnetic state cannot be reached by increasing the magnetic moment

from zero while gradually expanding the lattice: different atomic and electronic structures are characteristic of the two states, which are separated by an energy gap. The average per atom volume in the magnetic state is approximately 1 % larger compared to the nonmagnetic state, while this difference is mostly due to the expansion of the tetrahedra formed by four C atoms around the Fe atoms; this expansion was found to be reaching 10 volume percent. Furthermore, TM bond length changes turn out to be different for different carbon atoms in the tetrahedra around Fe impurities. The relaxation additionally depends on SiC polytype and lattice site the impurity substitutes at. For example, for Fe at the hexagonal site in 4H-SiC, the relaxation in the magnetic state strongly affects C atom which is above the Fe atom in the *c*-axis direction, while the other three atoms in the tetrahedron shift noticeably less. This is illustrated by Fig. 3 (b). At the cubic sites in 4H-SiC and in 3C-SiC (in 3C-SiC all lattice sites possess cubic symmetry) the relaxation is nearly equilateral and C atoms in the elemental tetrahedra around Fe atoms shift more or less the same distance. The inset in Fig. 3 (b) presents the details of the elemental tetrahedron relaxation for Fe substituting at the lattice sites with different symmetries in 4H- and 3C-SiC. We thus conclude that TM-impurity-induced lattice reconstruction, which self-consistently defines the electronic and magnetic configuration of the DMS, depends not only on TM atom's nearest neighbors, which are the same for all SiC polytypes and inequivalent lattice sites, but also noticeably on the long-range stacking sequence.

Total energy – supercell volume dependencies for Mn-, Cr-, and V-doped 3C-SiC are presented in Fig. 4. Similarly to the case of (Si, Fe) C, SiC DMSs with these substitutional impurities can again be in either the nonmagnetic or magnetic state. However, the relationship between the two states is the opposite of that in (Si, Fe) C with the magnetic state lying lower on the energy scale and thus being energetically favorable. At the equilibrium volume the energy gap between the two states changes from a small value of 12 meV/atom in the case of V doping to 18 meV/atom in (Si, Mn) C and 45 meV/atom in (Si, Cr) C. The higher the energy gap between the states, the more “stable” the magnetic state is against thermal fluctuations. If, as we suggest below, magnetic-nonmagnetic state mixing takes place at nonzero temperatures, the average magnetic moment in (Si, Cr) C may be expected to be closest to its calculated zero temperature value.

Magnetic moments as a function of the supercell volume behave in a different manner for V, Cr and Mn (see Fig. 5). While the former two change only slightly in the range of the average volumes from 68 to 78 a.u.³/atom, magnetic moment of Mn experiences a steep increase from 1.5 μ_B at 68 a.u.³/atom and then almost saturates at approximately 2.5 μ_B for the larger values of the atomic volume. Such behavior of the magnetic moments can be related to the differences in the nature of the electronic orbitals of the TM atoms, the degree of their hybridization with the surrounding dangling bonds and, therefore, to the influence of the electronic structure of the host lattice. The same factors influence relaxation of the lattice as it approaches equilibrium after the impurity substitution. For instance, in (Si, V) C and (Si, Cr) C, the relaxation is mostly absorbed by the tetrahedra of four carbon atoms around the TM impurity, similarly to the case of (Si, Fe) C. For Mn-doped SiC there are noticeable changes in Si atom positions in the layers other than impurity substitution layer. For all three impurities, the equilibrium average lattice volume is larger for the magnetic state of the crystal, compared to the nonmagnetic state, while in the nonmagnetic state relaxation is, again, small compared to pure SiC.

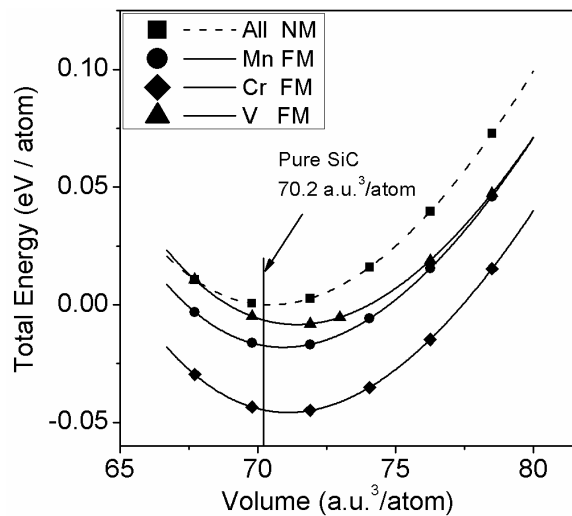


Fig. 4. Total energy – supercell volume dependencies for 3C-SiC doped with Mn, Cr, or V. The $E_{TOT}(V)$ curves for different impurities are brought to the same energy scale for easy comparison of the energies in the nonmagnetic and magnetic states.

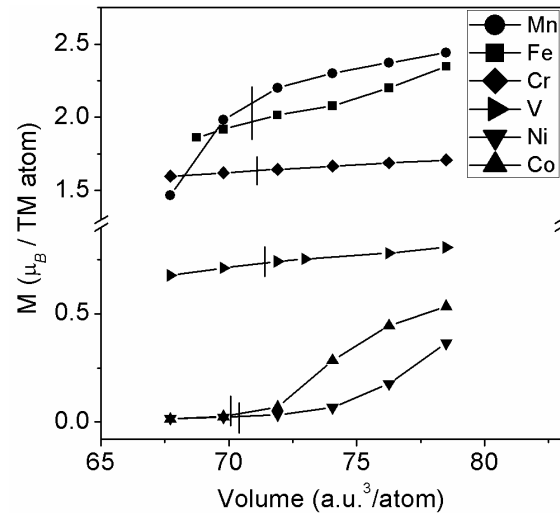


Fig. 5. Magnetic moment per impurity atom for different TM impurities substituting in 3C-SiC. Vertical lines mark equilibrium volume for each particular DMS.

Nickel and cobalt exhibit yet another behavior in the SiC matrix, different from that demonstrated by the other TM impurities. We found that for (Si, Co) C and (Si, Ni) C the magnetic and nonmagnetic solutions are very close on the energy scale. In the range of the supercell volumes from 68 to 78 a.u.³/atom the difference between the solutions is not greater than just a few meV/atom, which is close to the accuracy of our calculations, so that we can state that the two solutions coincide. Both (Si, Co) C and (Si, Ni) C are practically nonmagnetic in their equilibrium lattice configurations, with the magnetic moments of about $0.02 \mu_B$ /TM atom. The magnetic moments go up noticeably as (Si, Ni) C or (Si, Co) C lattice is expanded reaching almost $0.4 \mu_B$ /Ni and more than $0.5 \mu_B$ /Co at the average atomic volume of 78 a.u.³/atom (see Fig. 5). Thus, in the case of Co and Ni substitution, transition from the practically nonmagnetic to a magnetic state occurs gradually, in contrast to Mn, Cr, V, and Fe-doped SiC, where the two states are separated by a significant potential step/barrier. Average equilibrium per atom volumes for both Ni- and Co-doped SiC are practically equal to those of pure SiC, however, host lattice reconstruction due to Ni and Co substitution turns out to be rather pronounced. The expansion of the tetrahedra around the impurity atoms reaches 3% for (Si, Co) C and is as large as 10% in (Si, Ni) C at the equilibrium volumes. This local relaxation is compensated by the corresponding changes in other, primarily Si, atom positions so that the average per atom lattice volume remains almost equal to that in pure SiC. As the lattice of (Si, Ni) C or (Si, Co) C is further expanded away from the equilibrium, which is accompanied by the magnetic moment growth, the tetrahedra containing Co or Ni atoms expand even further, with their relative (to pure SiC with the same unit cell volume) volumes reaching 13% for Ni and 4% for Co at the average volume value of 78 a.u.³/atom. At the same time, relaxation of the rest of the supercell reduces with the Si atoms returning to the positions characteristic to pure material,

indicating that these atoms provide the supercell rigidity preventing the TM-C tetrahedra from expanding further and the TM atoms from possibly reaching the high-spin state.

TM species	$\Delta E_{\text{FM-NM}}$ (meV/atom)	M_0 (μ_B /TM)	M_A (μ_B /TM)
V	-12	0.74	0.45
Cr	-45	1.63	1.39
Mn	-18	2.09	1.39
Fe	33	1.92	0.42
Co	0	0.03	0.03
Ni	0	0.02	0.02

Table 1. Properties of TM-doped 3C-SiC: total energy differences between ferromagnetic and nonmagnetic states, $\Delta E_{\text{FM-NM}}$; magnetic moments at the equilibrium cell volume in the FM state, M_0 ; average over the states magnetic moment at room temperature and equilibrium cell volume, M_A , estimated assuming that the energy relationship between the FM and NM states remains the same as at zero temperature and using Boltzmann distribution function for calculation of the occupation probabilities.

3.2 Magnetic-nonmagnetic state relationship and mixing

Our calculations show that, similarly to what was known as a peculiarity of certain transition metals and alloys (Moruzzi & Markus, 1988; Moruzzi et al., 1989; Wassermann, 1991; Timoshevskii et al., 2004), TM-doped SiC can exist in one or another of the states differing in their structural and electronic properties, and in particular with the TM impurities possessing either zero or a nonzero magnetic moment. The states are characterized by significant differences in the lattice geometry, electronic density distribution, and thus chemical bond structure. As a result, coupling of the substitutional transition metal impurity electronic orbitals to the surrounding host atoms in the different states varies depending both on the substitution atom electronic structure and on the electronic configuration of the surrounding dangling bonds as well as more distant atoms in the lattice. In turn, substitution of a host atom by a TM atom results in SiC lattice reconstruction, which self-consistently defines the electronic and magnetic configuration of the impurity and SiC-TM DMS material. Transition between the different states can be gradual, such as in the case of (Si, Ni) C and (Si, Co) C, or the states can be separated by an energy gap – (Si, V) C, (Si, Fe) C, (Si, Mn) C, (Si, Cr) C, and the width of the gap varies for different impurities and SiC polytypes. It is not unreasonable to suggest that such multistate nature could also be peculiar to the other DMS material systems. Below in Fig. 6 we present partial densities of states for the nonmagnetic and magnetic configurations for the example of Mn-doped 3C-SiC. Clearly, the DOS spectra are completely different and while in the magnetic case the state filling is half-metallic with no occupancy in the minority spin channel, in the nonmagnetic case the DOS is not polarized at all and Mn d-electrons symmetrically fill the majority and minority states creating zero net magnetic moment. Below we provide a detailed analysis of DOS spectra of SiC doped with different TM impurities and deduce the exchange mechanisms responsible for the magnetic ordering in each particular case.

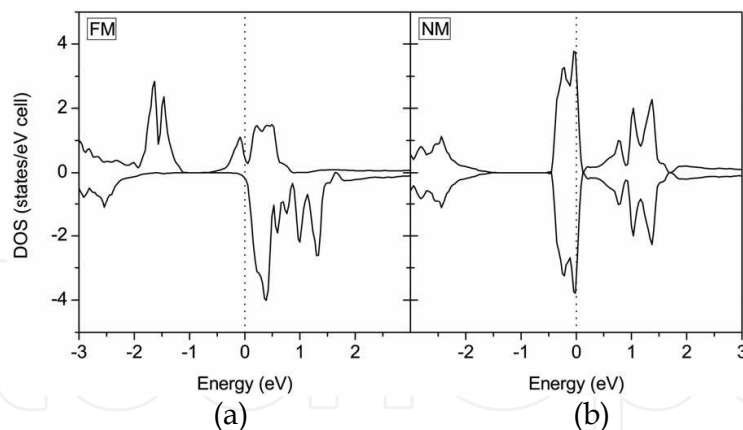


Fig. 6. Partial densities of states of Mn-doped 3C-SiC in its (a) ferromagnetic and (b) nonmagnetic states. Origin of the energy axis corresponds to the Fermi level position.

It is interesting to note that the magnetic state of SiC DMS is always realized in a lattice which is noticeably expanded compared to the nonmagnetic state (see discussion above), and one can therefore rather simplistically state that the TM atom “needs” more space for itself in the host lattice to acquire a magnetic moment. If the magnetic state is not the ground state of the DMS ((Si, Fe) C is an example), experimental realization of the magnetic state, which is a required prerequisite for spintronic device operation, may be achieved by either changing the lattice geometry in, for example, the lattice expanded due to ion implantation, or by making the magnetic state favourable by applying magnetic field under a high temperature equilibrium growth conditions. In the latter case, the magnetic state of the TM atoms leads to the corresponding lattice reconstruction, while nonequilibrium rapid lattice cooling to the point where the atom mobility is low could “freeze” the lattice in its magnetic state. If the magnetic state is the ground state it can of course be achieved under equilibrium growth conditions.

It is important to remember that calculations presented here were performed in the framework of the ground state density functional theory and describe SiC DMS material system at zero temperature conditions. At a nonzero temperature, the free energy of the crystal will additionally contain entropy terms with contributions due to both atomic position fluctuations and, in the magnetic case, due to the magnetic moment magnitude and direction fluctuations. Since configurational and magnetic fluctuations are due to similar thermal disordering processes, per atom values of the entropy terms quantifying fluctuations at these degrees of freedom of different nature should be of about the same order of magnitude. The experimental standard molar entropy values are equal to 16.5 J/mol K for hexagonal SiC and 16.6 J/mol K for cubic SiC (Lide, 2009). A simple estimate using these values yields the magnitude of the room temperature configuration disorder entropy of about 50 meV/atom. This exceeds the energy gap between the nonmagnetic and magnetic states for all impurities that we study and, consequently, at a high enough temperature the relationship between the two solutions can, in principle, change. This, for example, may lead to the magnetic state (ferromagnetic or antiferromagnetic) becoming energetically favourable, compared to the nonmagnetic state, in the case of Fe in SiC, for which the ground state solution is nonmagnetic. This possibility of changing the state preference may explain the magnetic response reported in several experimental studies of Fe-doped SiC (Theodoropoulou et al., 2002; Stromberg et al., 2006).

Furthermore, the fact that the magnetic and nonmagnetic solutions are separated by an energy gap comparable to room temperature thermal energy, allows us to suggest that a new equilibrium mixed state with a certain distribution of TM atoms between the magnetic and nonmagnetic states, and an average over this distribution magnetic moment, may be created at a nonzero temperature. Such state mixing may, in addition to other effects, explain the smaller, compared to calculated, values of the experimentally observed magnetic moments reported for GaN- and SiC-based DMS materials (Park et al., 2002; Lee et al., 2003; Singh et al., 2005; Bouziane et al., 2008). Somewhat similar mixed states can be realized in glasses where multiple unstable and easily thermally activated local atomic configurations exist. In these configurations atoms can occupy, with nearly equal probabilities, one of the several quasi-equilibrium positions and there exist a nonzero probability of tunneling transitions between these configurations (Anderson et al., 1972). If a mixed magnetic/nonmagnetic state is created, the average TM magnetic moments in this case will be lower compared to the purely magnetic case (Cf. Table 1). This leads to a reduction of the effective internal magnetic field stabilizing the magnetic order, which in turn means that the magnetic order will become weaker against thermal fluctuations or, equivalently, the mean-field Curie temperature will be reduced. Detailed analysis of the effects of state mixing and disorder is, however, rather involved and is beyond the scope of this study.

4. Magnetic ordering and critical temperatures

4.1 Magnetic coupling strength and range

We now turn to the calculations of the total energy of the ferromagnetic and antiferromagnetic states of the SiC-TM supercells containing a pair of TM atoms. We do not consider Co and Ni doping here, as magnetic moments of these impurities are practically zero at the equilibrium cell volume and are also rather small even in a significantly expanded lattice (Cf. Fig. 5). The strength of the exchange coupling and the values of the Curie or Néel temperature are estimated using the energy difference $\Delta E_{\text{FM-AFM}}$ between the FM and AFM states according to Eq. (1) above. We also note that the calculations of the total energy of the FM- and AFM-ordered supercells again, as in the case of magnetic moment calculations above, included a full inhomogeneous relaxation procedure. Since the FM and AFM states are in general characterized by different electronic density distribution and, self-consistently, atomic bond structure, we found accounting for the relaxation to be very important for an accurate calculation of the magnetic coupling strength and ordering temperatures. By separately relaxing the FM and AFM-ordered supercells we additionally find that magnetic moments in these two states are, in general, different.

SiC-TM FM-AFM energy differences and the corresponding values of the Curie or Néel temperature are summarized in Table 2 for TM substitution in 3C-SiC (supercells in Fig. 2 (a) and (b)). In the magnetic state, SiC DMS with substitutional Cr, Mn, and V orders ferromagnetically, while (Si, Fe) C orders antiferromagnetically. The strength and spatial extent of the exchange interaction vary significantly over the TM impurity range. For Cr the strength of magnetic coupling and, correspondingly, the Curie temperature drop from very high values in the nearest-neighbor arrangement to almost negligible values when the impurities are separated by two Si-C bilayers. There is even a change of sign and the interaction becomes antiferromagnetic in the latter case, however, such small FM-AFM energy difference values are comparable to the accuracy of our calculations and thus the

values of the coupling energy and the Curie temperature can safely be considered to be zero. In contrast to Cr, Mn impurity exchange interaction is, although somewhat weaker, less dependent on the distance between impurity atoms. Similarly to the stronger, compared to Cr, volume dependence of Mn magnetic moments, this can be explained by the fact that in the case of Mn, an additional d-electron starts filling the antibonding t_2 orbitals, the symmetry of which is the reason for their delocalized nature and longer range exchange interaction (see Fig. 7 and a detailed discussion below). On the contrary, in (Si, Cr) C d-electrons fill the strongly localized nonbonding e orbitals, which explains the short ranged albeit strong exchange in (Si, Cr) C DMS. Thus, for a reasonable impurity concentration of 5% and a uniform impurity distribution, the Curie temperature of Mn-doped 3C-SiC DMS reaches 316 K, which makes this material a good candidate for achieving room temperature DMS behaviour. In the nearest-neighbour arrangement, with a much shorter Mn-Mn distance, the Curie temperature of (Si, Mn) C is comparable to the former case, which can be justified by a different mutual orientation of the electronic orbitals of Mn atoms and also by the fact that there is an about 15% reduction of the magnetic moments of Mn atoms in this configuration. In the case of V, the latter effect is even stronger and magnetic moments are completely quenched for V atoms as the nearest neighbors, so that the material becomes nonmagnetic. As mentioned above, we found magnetic coupling energy $\Delta E_{\text{FM-AFM}}$ and the corresponding critical temperature values to be strongly dependent on the supercell relaxation in both the FM- and the AFM-aligned magnetic moments. The dependence is particularly strong in the cases where the exchange coupling is long-ranged, such as in (Si, Mn) C, while lattice relaxation involves a large number of supercell atoms, not just the nearest neighbours as in, for example, (Si, Fe) C or (Si, Cr) C. This once again points out the importance of accounting for lattice relaxation in the calculations of magnetic properties of TM-doped semiconductors.

TM species	$\Delta E_{\text{FM-AFM}}$ (meV/cell)		Mean-field T_C (K)	
	$d_{\text{TM}} = 14.27$ a.u.	$d_{\text{TM}} = 5.82$ a.u.	$d_{\text{TM}} = 14.27$ a.u.	$d_{\text{TM}} = 5.82$ a.u.
Cr	5	-222	-19	859
Mn	-82	-92	316	357
V	-23	0	88	0
Fe	107	221	-412	-854

Table 2. Total energy differences between the ferromagnetic and antiferromagnetic states $\Delta E_{\text{FM-AFM}}$ and mean-field values of the critical temperature T_C for TM-doped 3C-SiC, calculated using Eq. (1) for two different distances between TM impurities d_{TM} (Fig. 2. (a) and (b)). Negative $\Delta E_{\text{FM-AFM}}$ and positive T_C is characteristic of the FM ordering, while for AFM ordering $\Delta E_{\text{FM-AFM}}$ is positive and T_C is negative, the latter can be interpreted as the positive Néel temperature.

We also note that the exchange coupling energy values $\Delta E_{\text{FM-AFM}}$, although larger than the energy differences between the (ferro)magnetic and nonmagnetic states $\Delta E_{\text{FM-NM}}$ for the same impurities, cannot be compared to them directly. The exchange coupling energy, which is used in the corresponding mean-field Curie temperature expression, is the total energy difference between the FM- and AFM-ordered supercells containing a pair of TM

atoms. This is the amount of energy needed to flip the spin of one of these atoms and thus change magnetic ordering of the supercell from FM to AFM or vice versa; therefore, this energy is counted *per supercell*. The second quantity $\Delta E_{\text{FM-NM}}$ is the amount of total energy needed to reconstruct the entire supercell (or the entire crystalline lattice) in such a way that the TM atoms in this lattice acquire or lose their magnetic moments. The reconstruction involves every atom in the supercell or lattice and therefore this quantity is counted *per atom*. If both the FM-AFM and FM-NM energy differences are brought to the same scale (per atom or per supercell) for comparison, the first difference becomes in all cases smaller than the second, indicating that the FM-AFM energy difference can be thought of as an additional “small splitting” of the corresponding magnetic state. Therefore, while for example the antiferromagnetic state of Fe atoms is more favourable compared to the ferromagnetic state, the total energy corresponding to either the FM or the AFM state is still significantly larger compared to the nonmagnetic state, which makes the nonmagnetic state the ground state in (Si, Fe) C.

4.2 Mechanisms of exchange interaction in SiC-TM

Understanding the nature of exchange coupling in DMS is an important problem in magnetic materials. As has been pointed out in (Belhadji et al., 2007), certain characteristic features of the DMS densities of states can be used not only for identification of the exchange mechanisms responsible for magnetic coupling but also for predicting the coupling strength and range. Due to the interaction with the crystal field in a tetrahedral lattice environment, such as in 3C-SiC lattice (the symmetry of 4H-SiC is lower than that of 3C-SiC), substitutional TM impurity d-orbitals form the so-called e and t_2 states creating localized energy levels in the semiconductor forbidden band or resonances in one of the allowed bands. The e and t_2 states, due to the different spatial distributions of their electronic clouds, experience different degrees of hybridization with the surrounding dangling bonds and thus the electrons filling these states experience different degrees of localization. The nature of the states TM d-electrons fill will determine the strength and range of exchange interaction between the d-electrons. In order to illustrate the details of TM state occupation, we calculated partial densities of states of V, Cr, Mn, and Fe in 3C-SiC. The nature of the particular impurity states is easiest to analyze in this polytype due its purely tetrahedral symmetry. In the other polytypes, such as in 4H-SiC, the T_d symmetry breaks, however, due to the short range tetrahedral environment the states will still approximately have the e or t_2 character. Thus, the analysis we present below is applicable to 4H-SiC as well. Partial densities of states for different TM impurities in 3C-SiC showing the impurity states of different nature are presented in Fig. 7.

When V substitutes for Si in SiC lattice, two of the three d-electrons completely fill the bonding t_2 states, while there is another d-electron half-filling the majority e -states. In such situation, when the Fermi level is in the middle of an impurity band, the energy is gained by aligning atomic spins in parallel. This leads to broadening of this band and shifting of the weight of the electron distribution to lower energies. This is Zener’s double exchange mechanism which leads to ferromagnetism (Sato et al., 2004; Akai, 1998). The width of the impurity band and thus the energy gain due to double exchange scales as the square root of impurity concentration and is linear in the hopping matrix element between the neighbouring impurities. This square root dependence implies that the Curie temperature increases quickly already at small impurity concentrations and then almost saturates as a

function of impurity concentration. Another mechanism characteristic to the electronic structure of (Si, V) C DMS is hybridization between the e and t_2 states of the majority spin channel. This hybridization results in the filled e states shifting to lower energies. The resulting energy gain additionally stabilizes ferromagnetism by superexchange (Sato et al., 2004; Akai, 1998). This energy gain scales linearly with the impurity concentration and is proportional to the square of the hopping matrix element between the e and t_2 states, which is relatively small due to the localized nature of the e orbitals. An additional consideration following from the Heisenberg model is that rather small magnetic moment of V leads to a reduction of the exchange interaction between V atoms and, as a result, to a relatively small T_C . Localized nature of the nonbonding e -states is another reason for the reduction of T_C in (Si, V) C DMS.

In Cr-doped SiC there is an additional d-electron in the e -states and the Fermi level falls between the majority e and antibonding t_2 bands, the former being fully filled and the latter being empty. No energy can be gained by broadening the filled e impurity band and, therefore, double exchange is not important in this case. Hybridization between the e and t_2 states of the majority spin channel again, as in the case of (Si, V) C, results in the energy gain from filled e states shifting to lower energies and thus ferromagnetism is due to superexchange. The localized nature of the e orbitals and resulting quick fall-off of the exchange interaction with the TM-TM distance are the reasons for the strong concentration dependence of the ordering temperature in (Si, Cr) C (Miao & Lambrecht, 2006).

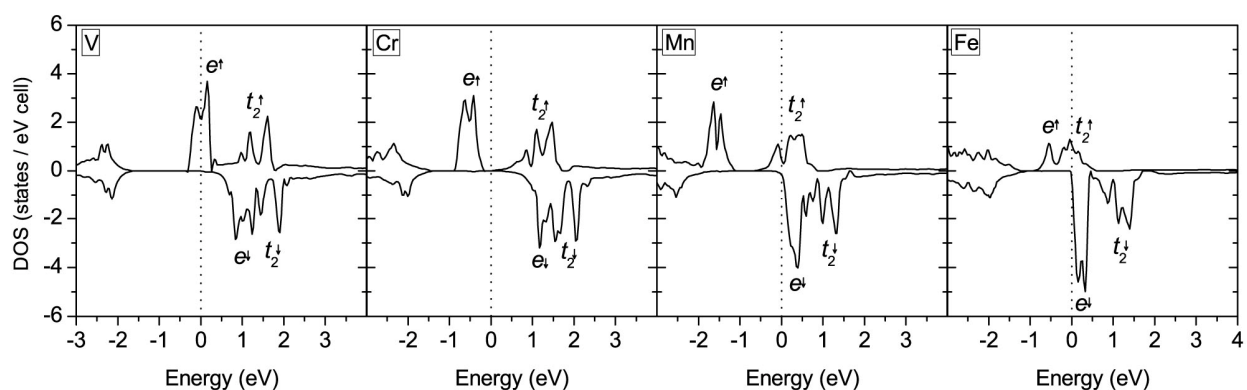


Fig. 7. Partial densities of states of TM impurities in 3C-SiC. Origin of the energy axis corresponds to the Fermi level position.

One more electron per TM in (Si, Mn) C is in the majority channel antibonding t_2 state and the Fermi level falls within the t_2 band. Thus, the double exchange kicks in again leading to ferromagnetism. Contrary to the case of (Si, V) C, however, the exchange interaction is between d-electrons in the less localized t_2 states, which results in a weaker TM-TM distance dependence and a more extended nature of the exchange. Ferromagnetic superexchange interaction due to the coupling between the majority e and almost empty t_2 states, although weaker than in (Si, Cr) C, because of the larger energy difference between these states, provides an additional stabilization of the ferromagnetic state in (Si, Mn) C. Another mechanism, which is characteristic to the electronic structure of (Si, Mn) C and which acts in competition with the double exchange, is the antiferromagnetic superexchange (Belhadji et al., 2007). The wave functions of the majority e and t_2 states hybridize with the antiferromagnetically aligned e and t_2 states of the opposite spin channel. As a result, the lower in energy states are shifted to even lower energies and the higher states are shifted to

higher energies. The energy is gained by reduction of the energy of filled states. The mechanisms of ferromagnetic and antiferromagnetic superexchange interactions are similar; whether the parallel or the anti-parallel alignment will be more energetically favourable depends on the strength of hybridization of states in the same and in the opposite spin channels. The double-exchange-stabilized ferromagnetic state is more favourable if the Fermi level lies well within the impurity band, while the energy gain due to superexchange is larger when the Fermi level lies between the bands of the same or opposite spin channels or near the band edges (Belhadji et al., 2007). In (Si, Mn) C, the hybridization of the majority and minority e states is weak because of their localized nature and relatively large energy difference between the two. Hybridization between the t_2 states is stronger, but only a small fraction of these states is filled, so in (Si, Mn) C double exchange wins stabilizing ferromagnetism.

In Fe-doped SiC, there is again a competition between the ferromagnetic double exchange and antiferromagnetic superexchange mechanisms. However in this case, the Fermi level is close to the top of the majority bands and separates the majority and minority bands. The energy gain due to double exchange is reduced because of the nearly complete filling of the antibonding majority t_2 band. At the same time, the superexchange becomes more dominant due to the stronger hybridization between the e and t_2 bands in different spin channels. This explains why (Si, Fe) C orders antiferromagnetically.

Recalling that the calculations are performed for the ground state of the DMS, we note that only direct exchange mechanisms can be accounted for in our model. At a nonzero temperature and if a sufficient concentration of free carriers is created in the DMS, carrier-mediated exchange can also be important. Depending on the concentrations of TM and other impurities and the details of the material atomic and electronic structure, different exchange channels may play different roles in stabilizing an ordered magnetic state. In particular, different free carrier and TM atom concentrations may result in RKKY-type exchange interactions of different signs and having an oscillating character depending on the distance between magnetic TM impurities. Contribution of this carrier-mediated exchange may favour ferromagnetic, antiferromagnetic or spin-glass-like order (the latter is, however, specific for nonuniform TM impurity distributions). The resulting effective magnetic ordering will depend on the relative strengths of the direct and carrier-mediated exchange interactions.

5. Room temperature ferromagnetism in Mn-doped SiC

Having identified Mn as the most promising doping choice for achieving room temperature ferromagnetism in SiC DMS, we now turn to a detailed investigation of magnetic properties of various “flavours” of (Si, Mn) C DMS, i.e. with Mn substituting in different SiC polytypes and at lattice sites with different symmetries thus producing different mutual spatial configurations of Mn atoms (and, consequently, of their magnetic moments). In addition to the supercells in Fig. 2 (a) and (b), for which this was done in the previous section, we calculate the total energy differences $\Delta E_{\text{FM-AFM}}$ between the FM- and AFM-aligned states and the corresponding Curie temperature values for the supercells shown in Fig. 2 (c-e). We then compare the results for all the 3C- and 4H-SiC crystal structures.

The results of the calculations are summarized in Table 3. One can see that for most of the configurations the strength of the exchange interaction is sufficient to lead to above room

temperature ferromagnetic ordering. As one could expect, there is a significant dependence of the exchange coupling strength on the substitution lattice site so that in some cases, such as for 4H-SiC with Mn atoms above each other in the c -axis direction (Fig. 2 (c)), the exchange is weaker although the impurity separation is relatively small. This lattice structure demonstrates the lowest Curie temperature, significantly below room temperature. Magnetic moments of substitutional Mn in this case are larger, closer to the atomic limit. For diagonally arranged impurities, either at the hexagonal or at the cubic sites in 4H-SiC (structures (d) and (e) in Fig. 2), exchange interaction becomes significantly stronger. In contrast to the 4H-SiC structure of Fig. 2 (c), in 3C-SiC the coupling between vertically arranged atoms (Fig. 2 (a)) is fairly strong with the corresponding value of the Curie temperature exceeding room temperature. According to the discussion above, Mn d -electrons in 3C-SiC occupy partially filled anti-bonding t_2 states. The symmetry of these states provides a significant coupling with the surrounding atoms and results in the extended range of exchange interaction between Mn atoms. This is in contrast to, for example, SiC-Cr, where d -electrons occupy strongly localized non-bonding e -states, while the anti-bonding t_2 states are empty, which leads to the very short-ranged albeit strong exchange and low Curie temperature. As already mentioned, although in 4H-SiC the T_d symmetry no longer applies, the d -states still have the e - or t_2 -like character and the particulars of their filling and local bonding remains the same.

SiC-TM crystal structure (Cf. Fig. 2)	Minimum distance between Mn atoms (a.u.)	$\Delta E_{\text{FM-AFM}}$ (meV/cell)	Mean-field T_C (K) (Eq. (1))	Magnetic moments FM/AFM (μ_B/Mn)
(a) 3C-SiC, impurities above each other	14.27	-82	316	2.18/2.05
(b) 3C-SiC, impurities as nearest neighbours in-plane	5.82	-92	357	1.70/1.53
(c) 4H-SiC, c -site, impurities above each other	9.59	-53	205	2.36/2.24
(d) 4H-SiC, c -site, diagonal impurity arrangement	11.61	-142	550	2.28/2.04
(e) 4H-SiC, h -site, diagonal impurity arrangement	10.18	-104	403	2.29/2.04

Table 3. Energy differences between the FM- and AFM-ordered supercells, the corresponding values of the Curie temperature and magnetic moments of Mn atoms in different configurations in 3C- and 4H-SiC.

Although the general rules apply both to 3C- and 4H-SiC, there still is a difference between the polytypes as becomes evident from the significant Curie temperature differences. Due to the different medium- and long-range order, the wave functions of Mn t_2 -like states, which are responsible for the exchange coupling between the TM atoms, are oriented differently with respect to each other in the different polytypes. Charge densities corresponding to Mn anti-bonding t_2 states in 3C-SiC, which were visualized in (Miao & Lambrecht, 2006), clearly illustrate that in this polytype d -electron wave function lobes are distributed approximately along the Mn bonds to the surrounding C atoms and extend significantly beyond the nearest

neighbours. Charge density isosurfaces of filled anti-bonding Mn states, corresponding to an equal value of this quantity, are shown in Fig. 8 for two different 4H-SiC FM-ordered supercells of Fig. 2 (c) and (d), demonstrating the smallest and largest ordering temperatures, respectively. Calculations show that the spatial distribution of these orbitals in 4H-SiC is somewhat different compared to 3C-SiC, with the more localized nature for the vertical impurity configuration (Fig. 2 (c)) explaining the lower value of the Curie temperature for this configuration in 4H-SiC despite the shorter distance between Mn atoms compared to the diagonal configuration (Fig. 2 (d)). The total energies of the supercells with the impurities substituting at the hexagonal sites are about 13 meV/atom lower compared to the case of the impurities at the cubic sites, making the former configuration more energetically favourable. However, in real DMS materials at high enough temperatures impurity atoms will be distributed among the sites with the hexagonal and cubic symmetries creating a new state with the magnetic properties averaged over the different configurations. As mentioned above, Mn-doped SiC can also exist in the nonmagnetic state, which is characterized by different crystal lattice structure and is at zero temperature separated from the magnetic state by an energy gap (Cf. Fig. 4). The energy gap is comparable to the thermal energy at room temperature and, therefore, the nonmagnetic state may also mix in at a nonzero temperature.

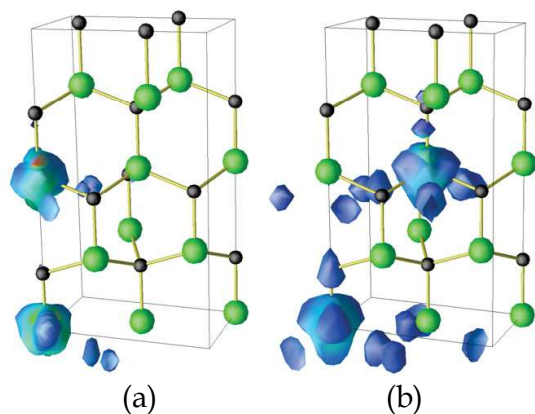


Fig. 8. Charge density isosurfaces for impurity states of Mn atoms substituting at quasicubic sites in 4H-SiC in (a) vertical and (b) diagonal configurations corresponding to the supercells shown in Fig. 2 (c) and (d).

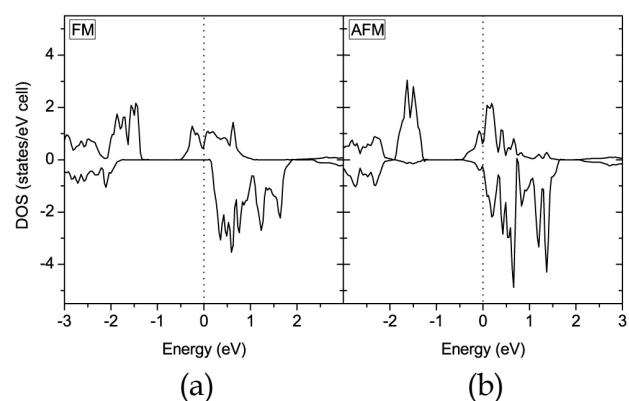


Fig. 9. Partial densities of states of Mn in 4H-SiC, calculated for the crystal structure shown in Fig. 2 (d) in its (a) ferromagnetic and (b) antiferromagnetic states. Origin of the energy axis corresponds to the Fermi level position.

Another interesting observation following from Table 3 is that Mn magnetic moments are in all cases smaller in the AFM-ordered supercells compared to the FM-ordered supercells. Relating this fact to the partial densities of states of Mn in the FM and AFM states shown in Fig. 9, one can conclude that in the AFM-ordered supercell the half-metallic behaviour is lost and the minority states become partially occupied, which leads to the reduction of the DOS polarization. Recalling the Heisenberg expressions for the energies of the FM and AFM states, one can perhaps also argue that the reduction of the magnetic moments in the AFM state and their increase in the FM state can be one of the factors stabilizing the FM state in the SiC-Mn DMS.

6. Concluding remarks and outlook

We presented a study of structural, electronic, and magnetic properties of SiC doped with first row transition metal impurities. For this we used density functional theory FLAPW calculation technique which is probably one of the most accurate first principles techniques to date. One of the primary results that we have established is that SiC DMSs can exist in either a magnetic or nonmagnetic state. The different states are characterized by substantially different equilibrium crystal lattice structures. Lattice reconstruction compared to pure SiC is typically significant when SiC DMSs are in the magnetic states, while in the nonmagnetic state the reconstruction is relatively minor. For V, Cr, Mn, and Fe doping the states are separated by an energy gap which needs to be overcome in order to change the state from nonmagnetic to magnetic and vice versa. At zero temperature, the magnetic state is energetically favourable in V-, Cr-, and Mn-doped SiC, while for Fe doping the nonmagnetic state is the ground state. The energy differences between the magnetic and nonmagnetic states vary from impurity to impurity and are also different in different SiC polytypes, being in many cases comparable to thermal energy at room temperature. On the other hand, in Ni- and Co-doped SiC the two states practically coincide, while the magnetic moments are close to zero in equilibrium lattice and gradually increase as the lattice is expanded. We argue that at a nonzero temperature the relationship between the two states of SiC DMSs can change due to the free energy entropy term. Furthermore, we speculate that a mix of the magnetic and nonmagnetic states is possible, which would change the average magnetic moment of the system and self-consistently its magnetic order. Such existence of multiple magnetic states may be peculiar to the other DMS material systems as well.

The values of magnetic moments, exchange interaction strength and range vary significantly across the range of impurities studied. While magnetic moments of Ni and Co grow noticeably starting from very small values at equilibrium unit cell volume, they are still rather small ($\sim 0.5 \mu_B$) even in a significantly expanded lattice. Even though the calculated lattice parameters correspond to zero temperature conditions, given the values of thermal expansion coefficient of SiC (Taylor & Jones, 1960), such larger lattice volumes cannot be reached by thermal expansion at practical temperatures. Thus Ni- and Co-doped SiC can be considered practically nonmagnetic and will likely not be suitable for spin injection or other spin-electronic applications. V, Cr, Mn, and Fe can exist in high-spin states in SiC matrix. We found that magnetic Fe in SiC orders antiferromagnetically, while the rest of the impurities order ferromagnetically. Small magnetic moments of V atoms and localized nature of d-orbitals in (Si, V) C prevent this DMS from reaching high ordering temperatures. Magnetic interaction between Cr atoms was found to be strong but short-ranged, so that (Si, Cr) C is also not expected to exhibit high ordering temperatures at reasonable Cr concentrations, at least if only the direct exchange mechanism is responsible for the ordering. On the other hand, Mn-Mn interaction, although not as strong, was found to be relatively weakly dependent on the interatomic distance. The resulting mean-field Curie temperature was estimated to be above room temperature even for the case of the relatively modest Mn doping of 5%. Exchange interaction was found to be strongly dependent on the spatial distribution of Mn in SiC lattice with the value of the Curie temperature reaching 550 K in one of the atomic configurations.

Given the long-range character of Mn-Mn exchange interaction in SiC host, among the TM impurities Mn is perhaps the most promising candidate for achieving room temperature

DMS behaviour. The analysis of the band structure of (Si, Mn) C suggests that ferromagnetic coupling in Mn-doped SiC is mostly due to Zener's double exchange, which is related to the fact that the Fermi level in (Si, Mn) C lies within a Mn impurity band in the gap. This result is reliable in the sense that there is no spurious resonance of Mn levels in the allowed bands. The latter is often a problem due to the notorious underestimation of the bandgap by DFT+LDA or DFT+GGA and, as a result, the source of a mistakenly assumed long-range carrier-mediated exchange in, for example, diluted magnetic oxides such as Mn-doped ZnO (Zunger et al., 2010 and references therein). Such incorrect placement of TM levels within the allowed bands leads to the creation of a hostlike delocalized orbital that promises long-range exchange interaction (similarly to the classic case of (Ga, Mn) As (MacDonald et al., 2005; Sato et al., 2010), where the highest Curie temperatures to date were confirmed for the "true DMS" material and where Mn impurities serve as a source of both magnetic moments and valence band holes, the latter mediating magnetic moment interaction via an RKKY-type Zener's kinetic p-d exchange mechanism). Thus, the electronic structure of (Si, Mn) C is rather different from that of (Ga, Mn) As and more resembling that of wide bandgap (Ga, Mn) N DMS (Sato et al., 2007) with the Fermi level within an impurity band in the gap. Still, however, we find the remarkably long range interaction between Mn atoms in SiC leading to the Curie temperature values being safely above room temperature.

It is of course important to keep in mind the approximations imposed by the use of the Heisenberg and mean-field models for the description of the SiC DMS system. In particular, many-electron effects, which may be important in the case of narrow impurity bands, if taken into account, may lead to an improvement of the Curie temperature estimations. For disordered systems one may need to additionally take into account the problem of exchange interaction percolation, as in this case the mean-field model tends to overestimate Curie temperature values for low impurity concentrations. Such overestimation, however, may not be as pronounced in the case of the longer-range exchange, which is demonstrated by substitutional Mn in SiC. On the other hand, introduction of free carriers in order to achieve free-carrier-mediated exchange, which is usually sufficiently long ranged and could further stabilize the FM state in SiC DMS, may only turn out possible by co-doping with a shallow impurity in addition to a TM, since TM levels in SiC are expected to be deep donors and acceptors (Miao & Lambrecht, 2006). Shallow impurity concentration will need to be comparable to the TM concentration to overcome compensation and produce a sufficient concentration of free carriers. This entails further reconstruction of the host lattice and is subject to solubility difficulties. Given the very high, compared to those typical to semiconductor devices, TM concentrations which are usually required for achieving the needed exchange coupling efficiency, one will likely need to resort to nonequilibrium growth and doping. Co-doping may become another alternative for increasing TM solubility (Pan et al., 2010). The strong influence of the substitution site and lattice relaxation on magnetic properties of SiC DMS also suggests that magnetic properties of such materials are expected to be very sensitive to the growth and processing conditions and point out the high importance of a careful experimental approach to their synthesis.

Rather scarce experimental data available for SiC DMSs do not, unfortunately, allow to judge conclusively on how accurate our predictions are. In a recent communication (Jin et al., 2008) 10% Cr-doped amorphous SiC was reported to be ferromagnetic above room temperature with the average magnetic moment of $0.27 \mu_B$. Although Cr concentration of 10% approximately corresponds to the $\text{Si}_7\text{C}_9\text{Cr}_2$ supercell for which we obtained a large

value of the ordering temperature, it should be kept in mind that effectively this result was obtained for the nearest neighbour dimers. As the magnetic interaction was found to drop off quickly beyond the nearest neighbours, for a random impurity distribution it would likely not percolate throughout the lattice. Although the authors reported their samples to exhibit hole conductivity, it may have been due to residual impurities or defects in the material since, according to the calculations (Miao & Lambrecht, 2006), both Cr donor and acceptor levels are deep in the gap and cannot be the source of free carriers. Nevertheless, the existence of free holes may have led to an additional, hole-mediated exchange interaction playing the role in stabilizing ferromagnetism at larger distances between the impurities. At least some of the experimental studies of Fe-doped SiC reported ferromagnetic DMS behaviour in Fe-implanted 6H-SiC (Theodoropoulou et al., 2002; Stromberg et al., 2006). Our calculations reveal nonmagnetic ground state and antiferromagnetic ordering in the magnetic state of (Si, Fe) C. Such discrepancy may be explained by several factors. First, as we already mentioned, state preference may change at nonzero temperatures. Second, our calculations were done for the TM impurities in the SiC lattice distributed either homogeneously or in the nearest neighbour pair configuration. Various other substitution TM configurations are possible and, as has been shown in (Cui et al., 2007) for (Ga, Cr) N DMS, different nanocluster complexes, including substitutional and interstitial TM atoms, as well as the other lattice defects, not only may be more favourable for formation compared to the homogeneous or random impurity distributions, but also can significantly alter magnetic properties of the DMS such as the ordering type and temperature. Various impurity complexes can coexist in a statistical distribution, further complicating the physical picture. Contribution of secondary phases to the magnetic signal can also not be ruled out completely (Stromberg et al., 2006).

SiC doped with Mn received more attention from the experimentalists compared to the other SiC DMSs and the reported promise of this impurity for obtaining high Curie temperatures is in-line with our conclusions. Most of the authors reported ferromagnetic ordering close to or above room temperature in Mn-doped SiC. These reports include ferromagnetism with the Curie temperatures of around 250 K in 5% Mn-implanted 6H-SiC (Theodoropoulou et al., 2002), low-Mn-doped polycrystalline 3C-SiC (Ma et al., 2007) and single crystalline 6H-SiC (Song et al., 2009). T_C around 300 K was reported for Mn-Si films synthesized on top of 4H-SiC and for Mn-diffused 3C-SiC (Wang et al., 2008). It should be stressed, however, that conclusions on the magnetic ordering and critical temperatures cannot be reliable if they are made using only magnetisation data, which is often the case. Lessons that have been learned in the last years suggest that the complex nature of DMS materials requires using a broad range of complementary techniques for an unambiguous all-around description of the material in-hand. Only such approach will allow avoiding possible pitfalls the experimentalist can encounter. Future theoretical work should also include studies of co-doping, impurity complexes and, perhaps, disorder to be able to provide an even more accurate guidance for the experimentalist. Recent detailed investigation of structural, magnetic and magneto-optical properties of thin Mn-doped SiC films (Wang et al., 2008) and investigation of Mn-defect complexes in 3C-SiC (Bouziane et al., 2008) are the first step towards understanding the nature of SiC DMSs, where impurities and defects constitute a significant portion of the crystal lattice atoms.

According to science historians, Wolfgang Pauli some 80 years ago said regarding impurities in semiconductors: "One shouldn't work on semiconductors, that's a filthy mess;

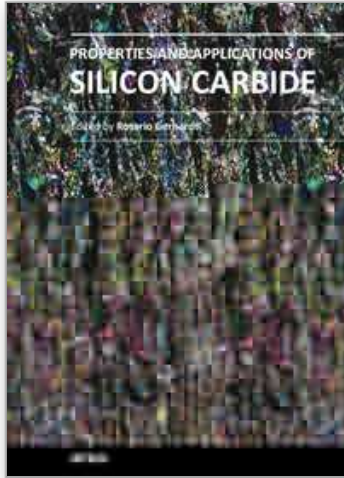
who knows whether any semiconductors exist." Modern semiconductor technology, which few these days can imagine the life without, managed to make an exquisite use of these once troublesome impurities. Will the researchers and technologists be able to continue the success story by integrating magnetism and harnessing the spin? We hope that the presented analysis of the magnetic states of SiC DMSs and the tendencies that were established may serve as a "road map" and motivation for experimentalists for implementing magnetism in silicon carbide, one of the oldest known semiconductors.

7. References

- Akai, H. (1998). Ferromagnetism and Its Stability in the Diluted Magnetic Semiconductor (In, Mn)As. *Phys. Rev. Lett.*, 81, pp. 3002-3005.
- Anderson, P.; Halperin, B. & Varma, C. (1972). Anomalous low-temperature thermal properties of glasses and spin glasses. *Philos. Mag.*, 25, pp. 1-9.
- Bechstedt, F.; Käckell, P.; Zywietz, A.; Karch, K.; Adolph, B.; Tenelsen, K. & Furthmüller, J. (1997). Polytypism and Properties of Silicon Carbide. *Phys. Status Solid, B*, 202, pp. 35-62.
- Belhadji, B.; Bergqvist, L.; Zeller, R.; Dederichs, P.; Sato, K. & Katayama-Yoshida, H. (2007). Trends of exchange interactions in dilute magnetic semiconductors. *J. Phys.: Condens. Matter*, 19, 436227.
- Bouziane, K.; Mamor, M.; Elzain, M.; Djemia, Ph. & Chérif, S. (2008). Defects and magnetic properties in Mn-implanted 3C-SiC epilayer on Si(100): Experiments and first-principles calculations. *Phys. Rev. B*, 78, 195305.
- Bratkovsky, A. (2008). Spintronic effects in metallic, semiconductor, metal-oxide and metal-semiconductor heterostructures. *Rep. Prog. Phys.*, 71, 026502.
- Cui, X.; Medvedeva, J.; Delley, B.; Freeman, A. & Stampfl, C. (2007). Spatial distribution and magnetism in poly-Cr-doped GaN from first principles. *Phys. Rev. B*, 75, 155205.
- Dewhurst, J.; Sharma, S. & Ambrosch-Draxl, C. (2004). <http://elk.sourceforge.net>.
- Dietl, T.; Ohno, H.; Matsukura, F.; Cibert, J.; & Ferrand, D. (2000). Zener Model Description of Ferromagnetism in Zinc-Blende Magnetic Semiconductor. *Science*, 287, pp 1019-1022.
- Dietl, T.; Ohno, H.; & Matsukura, F. (2001). Hole-mediated ferromagnetism in tetrahedrally coordinated semiconductors. *Phys. Rev. B* 63, 195205, pp 1-21.
- Gregg, J.; Petej, I.; Jouguelet, E. & Dennis, C. (2002). Spin electronics - a review. *J. Phys. D: Appl. Phys.*, 35, pp. R121-R155.
- Gubanov, V.; Boekema, C. & Fong, C. (2001). Electronic structure of cubic silicon-carbide doped by 3d magnetic ions. *Appl. Phys. Lett.*, 78, pp. 216-218.
- Hebard, A.; Rairigh, R.; Kelly, J.; Pearton, S.; Abernathy, C.; Chu, S.; & Wilson, R. G. (2004). Mining for high T_c ferromagnetism in ion-implanted dilute magnetic semiconductors. *J. Phys. D: Appl. Phys.*, 37, pp 511-517.
- Huang, Z. & Chen. Q. (2007). Magnetic properties of Cr-doped 6H-SiC single crystals. *J. Magn. Magn. Mater.*, 313, pp. 111-114.
- Jin, C.; Wu, X.; Zhuge, L.; Sha, Z.; & Hong, B. (2008). Electric and magnetic properties of Cr-doped SiC films grown by dual ion beam sputtering deposition. *J. Phys. D: Appl. Phys.*, 41, 035005.

- Kim, Y.; Kim, H.; Yu, B.; Choi, D. & Chung, Y. (2004). Ab Initio study of magnetic properties of SiC-based diluted magnetic semiconductors. *Key Engineering Materials*, 264-268, pp. 1237-1240.
- Kim, Y. & Chung, Y. (2005). Magnetic and Half-Metallic Properties Of Cr-Doped SiC. *IEEE Trans. Magnetics*, 41, pp. 2733-2735.
- Lee, J.; Lim, J.; Khim, Z.; Park, Y.; Pearton, S. & Chu, S. (2003). Magnetic and structural properties of Co, Cr, V ion-implanted GaN. *J. Appl. Phys.*, 93, pp. 4512-4516.
- Lide, D. (Editor). (2009). *CRC Handbook of Chemistry and Physics, 90th ed.* CRC, ISBN: 9781420090840, Boca Raton, FL.
- Ma, S.; Sun, Y.; Zhao, B.; Tong, P.; Zhu, X. & Song, W. (2007). Magnetic properties of Mn-doped cubic silicon carbide. *Physica B: Condensed Matter*, 394, pp. 122-126.
- MacDonald, A.; Schiffer, P. & Samarth, N. (2005). Ferromagnetic semiconductors: moving beyond (Ga,Mn)As. *Nature Materials*, 4, pp. 195-202.
- Miao, M. & Lambrecht, W. (2003). Magnetic properties of substitutional 3d transition metal impurities in silicon carbide. *Phys. Rev. B*, 68, 125204.
- Miao, M. & Lambrecht, W. (2006). Electronic structure and magnetic properties of transition-metal-doped 3C and 4H silicon carbide. *Phys. Rev. B*, 74, 235218.
- Moruzzi V. & Marcus, P. (1988). Magnetism in bcc 3d transition metals. *J. Appl. Phys.*, 64, pp. 5598-5600.
- Moruzzi, V.; Marcus, P. & Kubler, J. (1989). Magnetovolume instabilities and ferromagnetism versus antiferromagnetism in bulk fcc iron and manganese. *Phys. Rev. B*, 39, pp. 6957-6962.
- Munekata, H.; Ohno, H.; von Molnar, S.; Segmüller, A.; Chang, L.; & Esaki, L. (1989). Diluted magnetic III-V semiconductors. *Phys. Rev. Lett.*, 63, pp. 1849-1852.
- Olejník, K.; Owen, M.; Novák, V.; Mašek, J.; Irvine, A.; Wunderlich, J.; & Jungwirth, T. (2008). Enhanced annealing, high Curie temperature, and low-voltage gating in (Ga,Mn)As: A surface oxide control study. *Phys. Rev. B*, 78, 054403.
- Ohno, H.; Shen, A.; Matsukura, F.; Oiwa, A.; Endo, A.; Katsumoto, S.; & Iye, Y. (1996). (Ga,Mn)As: A new diluted magnetic semiconductor based on GaAs. *Appl. Phys. Lett.*, 69, pp. 363-365.
- Pan, H.; Zhang, Y-W.; Shenoy, V. & Gao, H. (2010). Controllable magnetic property of SiC by anion-cation codoping. *Appl. Phys. Lett.*, 96, 192510.
- Park, S.; Lee, H.; Cho, Y.; Jeong, S.; Cho, C. & Cho, S. (2002). Room-temperature ferromagnetism in Cr-doped GaN single crystals. *Appl. Phys. Lett.*, 80, pp. 4187-4189.
- Pashitskii E. & Ryabchenko S. (1979). Magnetic ordering in semiconductors with magnetic impurities. *Soviet. Phys. Solid State*, 21, pp. 322-323.
- Pearton, S.; Abernathy, C.; Overberg, M.; Thaler, G.; Norton, D.; Theodoropoulou, N.; Hebard, A.; Park, Y.; Ren, F.; Kim, J.; & Boatner, L. A. (2003). Wide band gap ferromagnetic semiconductors and oxides. *J. Appl. Phys.*, 93, pp 1-13.
- Perdew, J.; Burke, K. & Ernzerhof, M. (1996). Generalized Gradient Approximation Made Simple. *Phys. Rev. Lett.*, 77, pp. 3865-3868.
- Theodoropoulou, N.; Hebard, A.; Chu, S.; Overberg, M.; Abernathy, C.; Pearton, S.; Wilson, R.; Zavada, J.; & Park, Y. (2002). Magnetic and structural properties of Fe, Ni, and Mn-implanted SiC. *J. Vac. Sci. Technol.*, A 20, pp. 579-582.
- Sato, K.; Dederichs, P.; Katayama-Yoshida, H. & Kudrnovský, J. (2004). Exchange interactions in diluted magnetic semiconductors. *J. Phys.: Condens. Matter*, 16, pp. S5491-S5497.

- Sato, K.; Fukushima, T. & Katayama-Yoshida, H. (2007). Ferromagnetism and spinodal decomposition in dilute magnetic nitride semiconductors. *J. Phys.: Condens. Matter*, 19, 365212.
- Sato, K.; Bergqvist, L.; Kudrnovský, J.; Dederichs, P.; Eriksson, O.; Turek, I.; Sanyal, B.; Bouzerar, G.; Katayama-Yoshida, H.; Dinh, V.; Fukushima, T.; Kizaki, H. & Zeller, R. (2010). First-principles theory of dilute magnetic semiconductors. *Rev. Mod. Phys.*, 82, pp. 1633-1690.
- Seong, H.; Park, T.; Lee, S.; Lee, K.; Park, J.; & Choi, H. (2009). Magnetic Properties of Vanadium-Doped Silicon Carbide Nanowires. *Met. Mater. Int.*, 15, pp. 107-111.
- Shaposhnikov, V. & Sobolev, N. (2004). The electronic structure and magnetic properties of transition metal-doped silicon carbide. *J. Phys.: Condens. Matter*, 16, pp. 1761-1768.
- Sharma, S.; Dewhurst, J.; Lathiotakis, N. & Gross, E. (2008). Reduced density matrix functional for many-electron systems. *Phys. Rev. B*, 78, 201103.
- Singh, D.; Nordstrom, L. (2006). *Planewaves, Pseudopotentials, and the LAPW Method*, 2nd ed., Springer, ISBN: 978-0-387-28780-5, Berlin.
- Singh, R.; Wu, S.; Liu, H.; Gu, L.; Smith, D. & Newman, N. (2005). The role of Cr substitution on the ferromagnetic properties of $\text{Ga}_{1-x}\text{Cr}_x\text{N}$. *Appl. Phys. Lett.*, 86, 012504.
- Song, B.; Bao, H.; Li, H.; Lei, M.; Jian, J.; Han, J.; Zhang, X.; Meng, S.; Wang, W. & Chen, X. (2009). Magnetic properties of Mn-doped 6H-SiC. *Appl. Phys. Lett.*, 94, 102508.
- Story, T.; Gałazka, R.; Frankel, R. & Wolff, P. (1986). Carrier-concentration-induced ferromagnetism in PbSnMnTe. *Phys. Rev. Lett.*, 56, pp. 777-779.
- Stromberg, F.; Keune, W.; Chen, X.; Bedanta, S.; Reuther, H.; & Mücklich, A. (2006). The origin of ferromagnetism in ^{57}Fe ion-implanted semiconducting 6H-polytype silicon carbide. *J. Phys.: Condens. Matter*, 18, pp. 9881-9900.
- Syvjärvi, M.; Stanciu, V.; Izadifard, M.; Chen, W.; Buyanova, I.; Svedlindh, P.; & Yakimova, R. (2004). As-Grown 4H-SiC Epilayers with Magnetic Properties. *Mater. Sci. Forum*, 457-460, pp. 747-750.
- Taylor, A. & Jones, R. (1960). Silicon carbide (SiC), lattice parameters, thermal expansion, In: *Silicon Carbide - A High Temperature Semiconductor*, edited by J.R. O'Connor, J. Smiltens, pp.147-154, Pergamon Press, New York.
- Timoshevskii, A.; Yanchitsky, B. & Bakai, A. (2004). Composition dependence of the low-temperature magnetic ordering and the hyperfine interactions in Fe-N austenite. *Low Temperature Physics*, 30, pp. 469-478.
- Vinet, P.; Rose, J.; Ferrante, J. & Smith, J. (1989). Universal features of the equation of state of solids. *J. Phys.: Condens. Matter*, 1, pp. 1941-1963.
- Wang, W.; Takano, F.; Akinaga, H. & Ofuchi, H. (2007). Structural, magnetic, and magnetotransport properties of Mn-Si films synthesized on a 4H-SiC(0001) wafer. *Phys. Rev. B*, 75, 165323.
- Wang, W.; Takano, F.; Ofuchi, H. & Akinaga, H. (2008). Local structural, magnetic and magneto-optical properties of Mn-doped SiC films prepared on a 3C-SiC(001) wafer. *New Journal of Physics*, 10, 055006.
- Wassermann E. The Invar problem. (1991). *J. Magn. Magn. Mater.*, 100, pp. 346-362.
- Zunger, A.; Lany, S. & Raebiger, H. (2010). The quest for dilute ferromagnetism in semiconductors: Guides and misguides by theory. *Physics*, 3, 53.
- Žutić, I.; Fabian, J. & Das Sarma, S. Spintronics: Fundamentals and applications. (2004). *Rev. Mod. Phys.*, 76, pp. 323-410.



Properties and Applications of Silicon Carbide

Edited by Prof. Rosario Gerhardt

ISBN 978-953-307-201-2

Hard cover, 536 pages

Publisher InTech

Published online 04, April, 2011

Published in print edition April, 2011

In this book, we explore an eclectic mix of articles that highlight some new potential applications of SiC and different ways to achieve specific properties. Some articles describe well-established processing methods, while others highlight phase equilibria or machining methods. A resurgence of interest in the structural arena is evident, while new ways to utilize the interesting electromagnetic properties of SiC continue to increase.

How to reference

In order to correctly reference this scholarly work, feel free to copy and paste the following:

Andrei Los and Victor Los (2011). Magnetic Properties of Transition-Metal-Doped Silicon Carbide Diluted Magnetic Semiconductors, Properties and Applications of Silicon Carbide, Prof. Rosario Gerhardt (Ed.), ISBN: 978-953-307-201-2, InTech, Available from: <http://www.intechopen.com/books/properties-and-applications-of-silicon-carbide/magnetic-properties-of-transition-metal-doped-silicon-carbide-diluted-magnetic-semiconductors>

INTECH
open science | open minds

InTech Europe

University Campus STeP Ri
Slavka Krautzeka 83/A
51000 Rijeka, Croatia
Phone: +385 (51) 770 447
Fax: +385 (51) 686 166
www.intechopen.com

InTech China

Unit 405, Office Block, Hotel Equatorial Shanghai
No.65, Yan An Road (West), Shanghai, 200040, China
中国上海市延安西路65号上海国际贵都大饭店办公楼405单元
Phone: +86-21-62489820
Fax: +86-21-62489821

© 2011 The Author(s). Licensee IntechOpen. This chapter is distributed under the terms of the [Creative Commons Attribution-NonCommercial-ShareAlike-3.0 License](#), which permits use, distribution and reproduction for non-commercial purposes, provided the original is properly cited and derivative works building on this content are distributed under the same license.

IntechOpen

IntechOpen